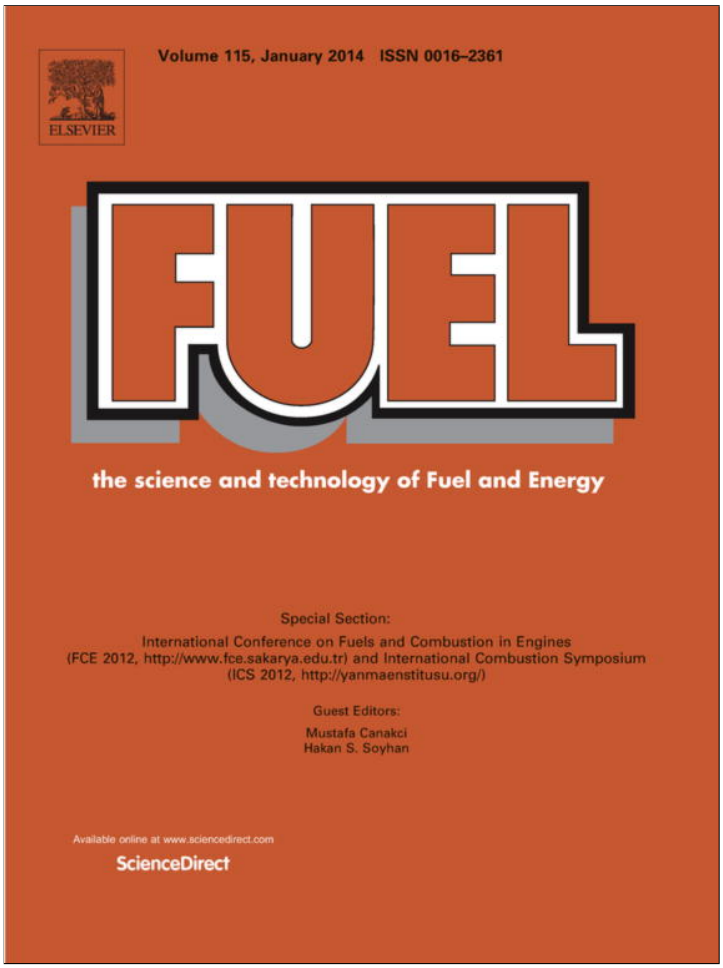

Fuel 115 (2014) 118–125

Contents lists available at SciVerse ScienceDirect

Fuel

journal homepage: www.elsevier.com/locate/fuel

Line shape analysis of the Raman spectra from pure and mixed biofuels esters compounds

Alisson M. Miranda [a,*], Eduardo W. Castilho-Almeida [b], Erlon H. Martins Ferreira [c], Gabriela F. Moreira [c], Carlos A. Achete [c], Raigna A.S.Z. Armond [c,d], Helio F. Dos Santos [b], Ado Jorio [a,*]

[a] Departamento de Física, Instituto de Ciências Exatas, Universidade Federal de Minas Gerais, CP 702, CEP 30161-970 Belo Horizonte, Minas Gerais, Brazil
[b] Departamento de Química, Universidade Federal de Juiz de Fora, CEP 36036-900 Juiz de Fora, Minas Gerais, Brazil
[c] Divisão de Metrologia de Materiais, Instituto Nacional de Metrologia, Qualidade e Tecnologia, CEP 25250-020 Xerem, Duque de Caxias, RJ, Brazil
[d] Departamento de Física, Universidade Federal de Uberlândia, CP 593, CEP 38400-902 Uberlândia, Minas Gerais, Brazil

HIGHLIGHTS

- Experimental spectra of biodiesel are fit based on theoretical calculations.
- The biodiesel ester composition can be determined using Raman spectroscopy.
- We derived a protocol to be used for determining the bio-origin of biodiesels.

ARTICLE INFO

Article history:
Received 21 April 2013
Received in revised form 17 June 2013
Accepted 25 June 2013
Available online 13 July 2013

Keywords:
Biodiesel
Fatty acid methyl esters
Raman spectra

ABSTRACT

This work provides a systematic and comprehensible lineshape analysis of the Raman spectra from (i) the main esters that compose the soybean biodiesel, namely Palmitate, Stearate, Oleate, Linoleate and Linolenate, (ii) mixtures of these esters, (iii) a soybean biodiesel reference material. Using theoretical spectral simulation as a guide, the experimental spectra are fit considering all the 3*N*-6 vibrational modes, where *N* is the number of atoms in the molecule. We demonstrate that while intensity analysis may lead to uncertainty in the definition of the relative ester contents in a mixture, a complete spectral analysis involving all parameters, including peak frequencies, allows spectral determination of esters composition. Finally we define a protocol that can be used for defining the specific composition of unknown, including adulterated biodiesels, important for quality control.

1. Introduction

The prediction of future oil scarcity and the unprecedented high rates of carbon emission in the atmosphere have forced society to seek for clean and renewable alternative energy resources, with particular emphasis given to biofuels [1–5]. The goal of this paper is to provide a systematic and comprehensible analysis of the Raman spectra of biodiesel.

Biodiesel is a clean, biodegradable, renewable, and nontoxic biofuel. It can be defined as monoalkyl esters derived from transesterification and hydro-esterification of vegetable oils, animal fats or waste oils with short-chain alcohols. It is composed of a mixture of several esters, which can be, usually, methyl or ethyl, saturated or unsaturated. This mixture of esters gives rise to important fuel properties in comparison to petrodiesel, such as relatively high lubricity, low sulfur content, high flash point and high cetane number values [6–10]. Several plants as well as its seeds, can be used as source of biodiesel, such as, soybean, canola, palm, crambe, macauba, castor, sunflower, olive and buriti [11]. The soybean oil is one of main raw material used to produce biodiesel [12]. The soybean biodiesel has its composition formed basically by five different esters: Palmitate, Stearate, Oleate, Linoleate and Linolenate [13]. For this reason, here we focus on the analysis of prepared mixtures of these esters, as the main components of the soybean based biofuels.

The molecular structures of methyl esters in biodiesel is varied, and so is their Raman spectra [8,14,15]. The main parameters are the total number of carbon atoms and of unsaturated carbons in the molecule. Esters are, therefore, named by these numbers, e.g. Methyl Linolenate is the (18:3), which means 18 carbons in the chain, with a total of 3 unsaturated carbon atoms [16].

Unlike other conventional methods of characterization, Raman spectroscopy is fast and simple, appropriated for *in situ* characterization. Beattie et al. [16] reported experimental measurements of Raman spectroscopy for the analysis of lipids: fatty acid methyl esters (FAME). An extensive discussion on the various parameters is presented, monitoring the number of carbons in a chain, number

* Corresponding author. Tel.: +55 3134096610.
E-mail addresses: alisson@fisica.ufmg.br (A.M. Miranda), adojorio@fisica.ufmg.br (A. Jorio).

0016-2361/$ - see front matter © 2013 Elsevier Ltd. All rights reserved.
http://dx.doi.org/10.1016/j.fuel.2013.06.038

of unsaturated carbons, liquid and solid phases, and *cis* vs. *trans* bond configuration. Ghesti et al. [14] used FT-Raman spectroscopy to monitor and quantify differences between the Raman spectra of pure soybean oil and ethyl esters. Zerbi et al. [17] studied the structural evolution with temperature of a few fatty acids using Raman and infrared spectroscopy. Calibration models based on multivariate analysis (PCR – Principal Component Regression, PLS – Partial Least Square Regression, ANN – Artificial Neural Network) were combined with FT-Raman and FT-NIR to quantify adulteration of biodiesel with vegetable oils and accuracies in biodiesel blends (principally B2 and B5) [18–20]. Guedes et al. [21] used absorption and emission spectroscopies to characterize oil samples obtained from buriti palm tree fruits. Farhad et al. [22] measured the Raman spectra of edible oils with an emphasis in the high-frequency 2800–3200 cm^{-1} region, enabling the measure and quantification of the unsaturations in edible oils. Lewis et al. [23] showed that a relative peak-height intensity ratio, I_{2850}/I_{2880}, serves as an index of the strength of the lateral interchain packing interactions. A decrease in this empirical peak-height intensity ratio reflects stronger lateral chain–chain interactions arising from a decrease in the spacing between lipid chains [23,24]. Brown et al. [25] determined the range I_{2890}/I_{2850} = 1.39–1.48 for liquid hydrocarbons while for the solids hydrocarbons the range was I_{2890}/I_{2850} = 1.61–1.72.

Theoretical studies of lipids compounds has been performed in order to establish the general rules which govern the relative energies of the conformers in short-chain FAME [26]. Density functional calculations have been used to investigate the conformations and Raman spectra of long-chain FAME [27]. Properties such as chain length and degree of unsaturation were determined.

Our work is distinguished as the search for the complete set of parameters that reveal the bands that make up the line shape of the Raman spectra of esters, mixtures of esters and real biodiesels. This paper is organized as follows: Section 2 presents the experimental and theoretical details; Section 3 presents the experimental results: in Section 3.1 the Raman spectra of pure esters are detailed; in Section 3.2 the mixture of esters and the Raman spectra of soybeam biodiesel are discussed, including a comparison of prepared mixtures with real soybean biodiesel; in Section 3.3 a protocol for analyzing the Raman spectra of a unknown soybean biodiesel is discussed, including possible routes for treating an adulterated sample; in Section 4 we present our conclusions.

2. Methodology

2.1. Sample details

Table 1 lists the methyl esters used in this study, (16:0), (18:0), (18:1), (18:2) and (18:3), chosen for being the main components of the soybean biodiesel, plus the (12:0) and (14:0), chosen as references for saturated esters that are liquid at room temperature. Methyl esters of high purity (99 + *m*/*m*%) provided from Aldrich®- were kept refrigerated for sample conservation. The measurements were performed with the esters at room temperature. The (16:0) and the (18:0) are solid (powder) at room temperature. For the (16:0) and (18:0), both solid and liquid phases were measured, where in the later case the temperature was raised up until reaching the melting point (T = 30.5 °C for the (16:0) and T = 39 °C for the (18:0))[28].

Different mixtures of the pure esters (Table 1) were prepared, as displayed in the first five lines of Table 2. The mixtures were obtained by the addition of pure ester to an amber glass bottle and prepared by weighting using a analytical balance (Mettler Toledo AB265-S, ±0.01 mg). The mixtures were homogenized using a Mixer (approximately 10 s) and an ultrasonic bath (30 min). Esters were combined ranging from binary mixtures to quaternary mixtures. In the last two lines of Table 2 we present the composition of soybean biodiesels. The first is a reference material (SRM 2772) [29] provided by the National Institute of Standards and Technology (SB-NIST) in collaborative work with the Instituto Nacional de Metrologia, Qualidade e Tecnologia (Inmetro). The mixture "SB-like" was produced with ester compositions similar to the SB-NIST standard. The second, mixture "SB-UNKN" is a sample of pure soybean biodiesel with ester compositions initially unknown. The reference and the "unknown" samples will be used here to discuss the protocol for determining ester composition, as well as adulterations in biodiesel. The methyl ester content of the "SB-UNKN" sample was independently determined by chromatography, in accordance with the EN 14103:2011 standard.

Finally, five mixtures of adulterated biodiesel were prepared by adding soybean oil in the SB-UNKN sample, as displayed in Table 3. The mixtures were prepared on an amber glass bottle using an analytical balance (Mettler Toledo AB265-S, ±0.01 mg). The mixtures were homogenized using both a Mixer (approximately 10 s) and an ultrasonic bath (30 min).

2.2. Spectra acquisition

The Raman spectra of pure esters, mixtures and biodiesel were measured in two systems: (1) a Horiba T64000 Raman spectrometer, equipped with a coupled charged detector (CCD) cooled with liquid N_2 and excited with an argon laser at 514.5 nm (2.41 eV), with power of (25.7 ± 0.1) mW; (2) a "home built" system using a spectrometer *Andor*TM Tecnology-Sharmrock sr-303i equipped with a coupled charged detector (*Andor*™ Technology-iDus Spectroscopy CCD) excited with a He–Ne laser (17 mW) at 632.8 nm (1.96 eV). Both systems are equiped with 600 groves/mm diffraction gratings. For each spectrum, 5 accumulations were added, 30 s each. The spectra were obtained in the 400–3800 cm^{-1} range, where we observe several first and higher-order Raman bands. An Hg lamp was used to calibrate the spectra.

Table 1
Pure methyl esters and their nomenclatures, according to (*n*:*m*), where *n* is total number of carbon atoms in the chain and *m* is the total number of unsaturated carbon–carbon bonds [28].

Ester	(*n*:*m*)
Methyl laureate	12:0
Methyl myristate	14:0
Methyl palmitate	16:0
Methyl stearate	18:0
Methyl oleate	18:1
Methyl linoleate	18:2
Methyl linolenate	18:3

Table 2
Mixtures of esters studied in this work and their compositions in percentage (±0.1%*w*/*w*). The last two lines bring the composition in percentage of two biodiesels, first a well defined reference material provided by NIST (SB-NIST), and second an initially unknown biodiesel (SB-UNKN), the percentages provided here being defined in this work by chromatography, in accordance with the EN 14103:2011 standard (±0.01%*w*/*w*).

Mixtures	(16:0)	(18:0)	(18:1)	(18:2)	(18:3)	(others)
35 × 65	35.0	–	65.0	–	–	–
2 × 50	49.8	–	–	50.2	–	–
25 × 45 × 30	24.8	–	45.1	30.1	–	–
4 × 25	24.8	–	24.7	25.0	25.4	–
SB-like	11.2	04.7	23.6	52.5	08.1	–
SB-NIST	10.70	04.30	23.30	52.30	07.82	01.58
SB-UNKN	9.57	2.71	25.74	47.84	3.69	10.45

Table 3
Percentage compositions (±0.1%*w*/*w*) of SB-UNKN adulterated by the addition of soybean oil.

Mixtures	(M1)	(M2)	(M3)	(M4)	(M5)
SB-UNKN	100.0	94.9	89.3	78.8	0.0
Soybean oil	0.0	5.1	10.7	21.2	100.0

2.3. Theoretical guide and experimental fitting

The baselines in the Raman spectra were subtracted using the software Peak Fit. In the same software, a sum of Lorentzian functions were used to fit the spectra. The number of peaks (Lorentzian functions) used to fit the Raman spectra is given by 3*N*-6, where *N* is the number of atoms in the molecule. Since *N* is usually large [*N* = 153 for the (16:0), 171 for the (18:0), 165 for the (18:1), 156 for the (18:2) and 153 for the (18:3)], we need a guide to help defining the number of peaks that should be used to fit each band in the spectrum. For this reason, we performed a computer simulation of the Raman spectra for each ester in Table 1. These molecules were initially subjected to molecular dynamics (MD) calculations, using the software package MacroModel [30], with the AMBER [31,32] force field, according to a heating protocol suitable for such molecules, seeking for a relaxation of the molecular structure. The structures selected by MD were then optimized at the level of theory SVWN/6-31G, following the methodology DFT implemented in the package Gaussian 03 [33,34]. After, calculations of harmonic frequencies and vibrational intensities were obtained using the same level of theory applied to the optimization of structures. Theoretical spectra can be built using the computational packages SIMULAT2 [35]. Finally, the experimental spectra were fit using the theoretical spectra as a guide. The frequencies and intensities were allowed to change freely in the fitting procedure, while the peak widths were shared to avoid divergence.

3. Results

3.1. Pure methyl esters

Fig. 1 shows the Raman spectra for the (18:1) in the region between 400 and 3800 cm^{-1}, obtained experimentally (top) and theoretically (bottom). There are some discrepancies between the experimental and theoretical spectra, such as the C═O and C═C stretching vibrations being calculated essentially with the same wavenumbers (1724.33 and 1724.85 cm^{-1}), thus overlapped within the band near 1720 cm^{-1}, while in the experiment they are well separated in frequency (see Fig. 1). However, the general agreement is good enough for our purposes. Articles [16,24,25,36,37] and books [38,39] already provide the general assignments for these spectroscopic signatures for esters. Accordingly, the several bands due to C_1–C_2 stretching, CH_3 rocking and C—O stretching (800–900 cm^{-1}), ═C—H bending (twisting between 900 and 1000 cm^{-1}), skeletal C—C stretching (1050–1150 cm^{-1}), ═C—H bending (scissoring between 1245 and 1277 cm^{-1}), CH_2 bending (twisting between 1290 and 1320 cm^{-1} and wagging between 1350 and 1380 cm^{-1}), CH_2 and CH_3 bending (1400–1500 cm^{-1}), C═C stretching (1600–1700 cm^{-1}), C═O stretching (1700–1750 cm^{-1}), C—H stretching vibrations (2800–3000 cm^{-1}) and olefinic ═C—H stretching symmetric and asymmetric (3000–3100 cm^{-1}) are indicated in Fig. 1.

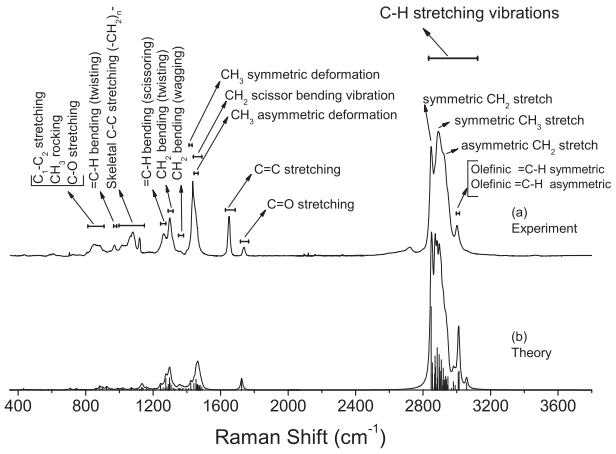

Fig. 1. Experimental (top) and theoretical (bottom) Raman spectra for the (18:1) methyl ester. Each vertical line in the theoretical spectrum indicates the frequency and intensity for one specific vibrational mode. We used $\gamma = 15\ cm^{-1}$ for the peak full-width at half maximum (FWHM) to build the theoretical spectrum that better resembles the experimental spectrum. 1 and 2 in C_1–C_2 represent the first and the second carbons in the molecular structure of the ester near the terminal C—C(═O).

The C—C stretch mode due to the terminal C—C(═O), appearing in the 800–900 cm^{-1} range, is assumed to be uncoupled from the C—C stretch modes of hydrocarbon chain skeleton, which occurs in the 1050–1150 cm^{-1} range [25]. Therefore, the way it is commonly defined in the literature, the vibrational mode frequency signatures have available windows, some reaching 100 cm^{-1}, making it difficult to study the specific nature of the many peaks that make up the Raman bands. All these bands comprising the Raman spectrum of biodiesel carry the characteristics of many different vibrational modes, as shown by the vertical lines in the theoretical spectrum (see Fig. 1 – bottom), and here we will provide a detailed experimental analysis of these characteristics.

Fig. 2 shows the Raman spectra for the main esters present in soybean biodiesel, as listed in Table 1, plus the (12:0) and (14:0), which are references for the analysis of unsaturated esters in the liquid phase. Differences are observed in the Raman intensities and frequencies of some bands due to several factors, including: liquid vs. solid phases [16,25], number of carbon atoms in the chains [16,26,27] and number of insaturations [16]. The line shape of a biodiesel Raman spectrum is determined by the relative amount of these esters. Therefore, information regarding each of these esters separately is important in the characterization and understanding of biodiesel spectra.

3.1.1. Liquid vs. solid phase and dependency on the number of carbon atoms in the chains

Fig. 3a compares the liquid and solid spectra for the (16:0), in the region between 650 and 3200 cm^{-1}. For this analysis, we used

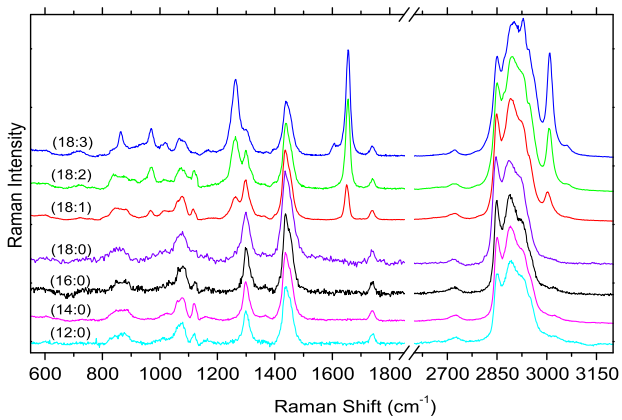

Fig. 2. Raman spectra for the pure esters (12:0), (14:0), (16:0), (18:0), (18:1), (18:2) and (18:3). The spectra were normalized based on the C═O stretching at 1740 cm^{-1}. For the (16:0) and (18:0), the liquid phase spectrum is shown after subtracting the temperature induced effect, as discussed in Section 3.1.1.

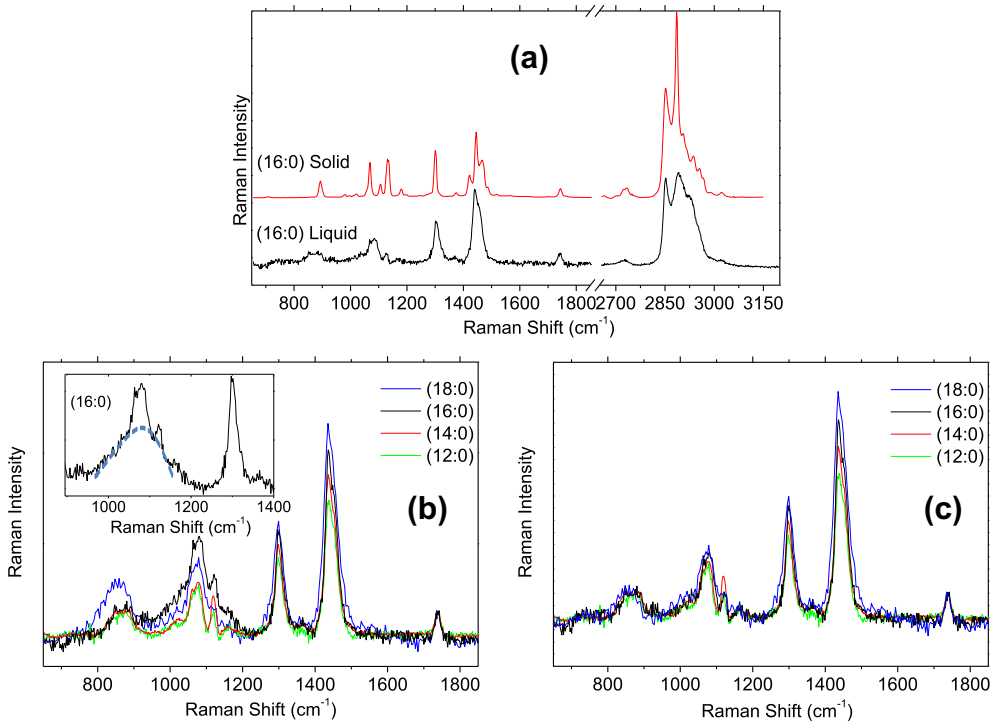

Fig. 3. (a) Raman spectra of the (16:0) in the solid (top) and liquid (bottom) phases in the regions between 650–1850 and 2650–3200 cm^{-1}. The spectra are normalized based on the stretching vibration of C=O at 1740 cm^{-1}. (b) Raman spectra of fully saturated esters (12:0), (14:0), (16:0) and (18:0) in the liquid phase. The inset to (b) shows a curve of correction for the high temperature induced background for the (16:0) and (18:0) in high temperature. (c) Raman spectra of the saturated esters (12:0), (14:0), (16:0) and (18:0) with intensity correction applied to the (16:0) and (18:0).

the methyl palmitate (16:0), solid at room temperature and liquid above 30.5 °C. Fitting these spectra with 3*N*-6 Lorentzians (not shown here, discussed in the next section) gives full width at half maximum (FWHM) equals to 7 ± 1 cm^{-1} in samples in the liquid phase, and 3 ± 1 cm^{-1} in samples in the solid phase. For liquid components, the individual peaks are broader and the bands tend to mix, making it more difficult to identify each peak intensity, width and position. The peaks become better defined in the solid material, allowing a better identification of each vibrational mode. In general, there are shifts in frequencies when comparing solid and liquid components. The Raman spectra of samples in the solid phase show sharp bands due the highly ordered hydrocarbon chains [23–25,37].

Fig. 3b compares the Raman spectra of the fully saturated esters: (*n*:0), *n* = 12, 14, 16, 18. For these esters the observed differences will be related only to the differences in the total number of carbons and hydrogens in the molecules. Increase in some Raman peaks intensity is observed, particularly in the regions of the spectrum regarding —CH_2-bending, especially for modes with frequencies around 1300 cm^{-1} and 1450 cm^{-1}. Note the absence of the band at 1650 cm^{-1} related to the C=C double bond stretching, characteristic of unsaturated esters. For the (16:0) and (18:0), the region between 800 cm^{-1} and 1200 cm^{-1} presents a broad feature, differentiating the high temperature (16:0) and (18:0) liquid phase spectra from the room temperature (12:0) and (14:0) spectra, due to the temperature increase to achieve the (16:0) and (18:0) melting points. A background was subtracted (inset in Fig. 3b) in the (16:0) and (18:0) for matching the (12:0) and (14:0) reference spectra (Fig. 3c). This procedure is needed because of the rise in temperature, causing variations in the relative intensities of the peaks. This effect is major in bands due to the skeletal C—C stretch, i.e. between 800 and 1200 cm^{-1}. Beattie et al. [16] showed the effect of temperature on the intensity of the C_1–C_2 band between 800 and 900 cm^{-1}.

3.1.2. Spectral dependence on the number of unsaturations

Fig. 4 shows the experimental [(a), (c) and (e)] and simulated [(b), (d) and (f)] Raman spectra of three types of esters, all with 18 carbons (18:*m*), with *m* = 1, 2, 3. Attention is given to the effect of increasing the number of double bonds (unsaturated carbons) in the molecules: oleate (18:1), linoleate (18:2) and linolenate (18:3). Unsaturated biodiesel spectra exhibit characteristic bands, such as the =C—H deformation vibration near 970 cm^{-1}, the =C—H deformation vibration near 1265 cm^{-1}, the C=C stretching vibration near 1650 cm^{-1} and =CH stretching vibration (CH olefinic) near 3000 cm^{-1}. The relative intensities of the bands near 970,1265,1650 cm^{-1} and 3000 cm^{-1} are proportional to the number of double bonds in the molecule. These bands are absent in the fully saturated components (*n*:0), as shown in Figs. 2 and 3. These differences make it possible to find correlations between the number of unsaturated carbons and the relative Raman peak intensities [16]. Relative frequency shifts can also occur depending on the number of unsaturations, as discussed later. The increase of double bonds C=C, i.e. one for the (18:1), two for the (18:2) and three for the (18:3), leads to a decrease in the number of C—C and CH_2 bonds in the molecules. Note the decrease of the peak intensities at ~1300 cm^{-1} and between 1400 and 1500 cm^{-1} for the (18:3). The peaks at ~860 cm^{-1} become more intense and sharp. Some remarkable changes occur in the region between 900 and 1100 cm^{-1}. The peak at 970 cm^{-1} increases with increasing the number of unsaturations. The opposite is observed for the peak at 1080 cm^{-1}. Similar effect occur in the regions between 1265 and 1305 cm^{-1} and between 1450 and 1650 cm^{-1}.

The fitting of the experimental spectra based on the simulated spectra provides more details for understanding these bands and their variations. In the region between 1400 and 1500 cm^{-1} there are several vibrational modes related to the angular deformation of the several CH_2. In this region there is a variation of the number of peaks, 17 for the (18:3), 18 for the (18:2), 19 for the (18:1) and

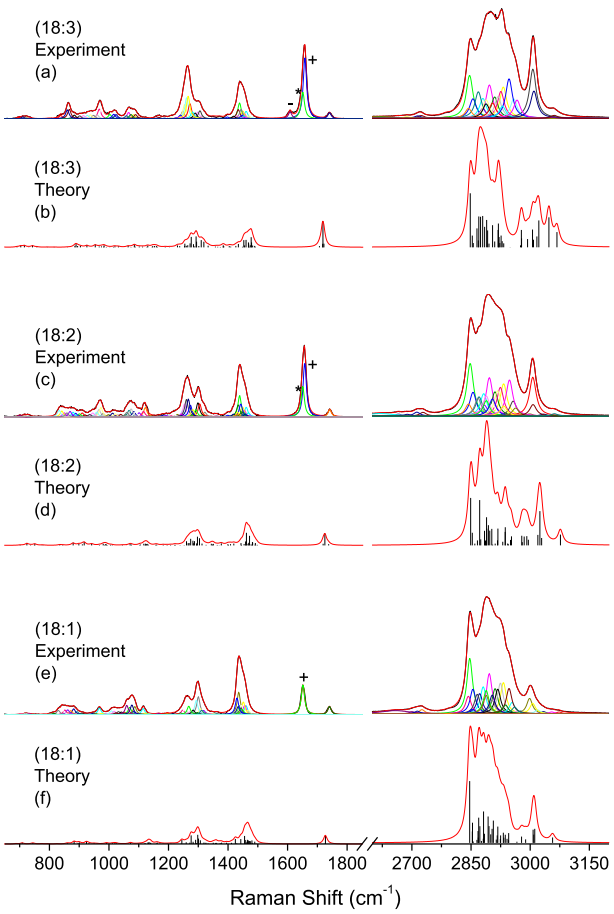

Fig. 4. Experimental [(a), (c) and (e)] and simulated [(b), (d) and (f)] Raman spectra of the (18:1), (18:2) and (18:3) pure esters. The Lorentzian curves used to fit the experimental spectra are shown. For the simulated spectra, the vertical lines give the calculated frequencies and relative intensities. The symbols "+", "*" and "–" indicate linear C=C stretching vibrational mode assignments, as given in Fig. 5.

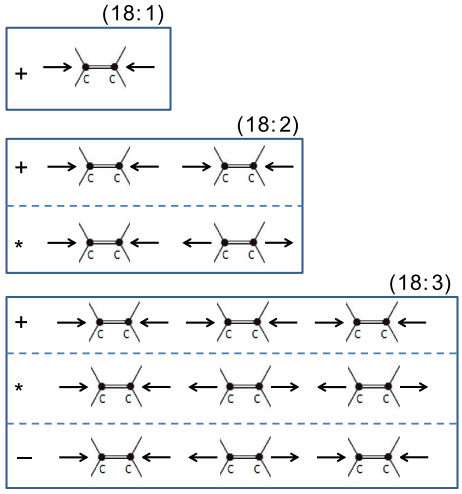

Fig. 5. Vibrational modes for the C=C bonds present in the (18:1), (18:2) and (18:3) esters. The symbols "+", "*" and "–" label the C=C vibration symmetries, and are used to assign the respective Raman peaks in Fig. 4.

21 for the (18:0). This is responsible for the variation of Raman intensity in this spectral region. In our fitting procedure, we searched for a correspondence between the peaks predicted by theory and the Lorentzian functions found in the experimental fitting analysis. Because theory is based on harmonic approximations for the calculations of the energies, it does not predict the frequencies accurately. For example, there is a clear discrepancy between the experimental and theoretical frequencies for the stretching bands C=O and C=C, as shown in Fig. 4 in the region between 1600 cm^{-1} and 1800 cm^{-1}. Fig. 5 shows the in phase and out of phase vibrational modes associated with the vibrations of 1, 2 and 3 C=C bonds in the esters (18:1), (18:2) and (18:3). *m* linear C=C stretching normal modes are expected and present in the esters (18:*m*). The up to 3 C=C vibrational modes and the C=O vibration are very close in frequency in the theoretical spectra ((b), (d) and (f) in Fig. 4) and exhibit a larger frequency spread in the experimental spectra ((a), (c), and (e) in Fig. 4). However, the relative peak intensities allows us to identify each mode in the experimental analysis, as given in Figs. 4 and 5 by the "+" , "*" and "–" symbols. Therefore, although theory is not accurate, it does provide a guide for spectral fitting using the full set of expected normal modes.

3.2. Mixed methyl esters

3.2.1. Binary mixture: the number of insaturations

Fig. 6 compares the experimental Raman spectra from the (18:1) with the mixture 2 × 50 (see Table 2) with 50% (18:2) and 50% (16:0). Both the pure (18:1) and the (16:0) + (18:2) mixture have on average one unsaturation per molecule. This is consistent with the similar intensities of the peaks at 1650 cm^{-1} and 3000 cm^{-1} for these two samples. However, there are differences in the peak frequencies. In Fig. 6a and b, the C=C stretching vibration and the CH olefinic vibration do not match in frequency. See inset to Fig. 6a ($\triangle\omega = 4 \pm 1$) cm^{-1} near 1650 cm^{-1} and Fig. 6b ($\triangle\omega = 6 \pm 1$) cm^{-1} near 3000 cm^{-1}. This shift is due to the fact that the (18:2) in the mixture (16:0) + (18:2) shows two C=C stretching related vibration modes, and the frequencies do not match exactly with the one from the (18:1) (see Figs. 4 and 5). In the 1050–1150 cm^{-1}, 1290–1320 cm^{-1} and 1400–1500 cm^{-1} frequency ranges, the intensities do not perfectly match due to differences in the chain length. While the (18:1) contains 18 carbon atoms, the mixture (16:0) + (18:2) contains 17 carbon atoms per molecule. These changes are perceptible in the spectrum of the mixture.

3.2.2. Mixture of more than two esters

In a spectrum of mixed esters, the Lorentzian based fittings should include the individual modes of each ester in the mixture. In a mixture with five esters, for example, (16:0), (18:0), (18:1), (18:2) and (18:3), six modes are expected in the region between 1600 cm^{-1} and 1700 cm^{-1} (shown in Fig. 5). Knowing the pure esters constituents, it is possible to determine the spectrum of the mixture through a weighted average, by considering the proportion of each ester in the mixture. The intensities in the blends can be represented by

$$I(\omega) = \sum_{n,m} M_{n:m} I_{n:m}(\omega), \quad (1)$$

where $I(\omega)$ and $I_{n:m}(\omega)$ are the total spectral intensity and the intensity for the (n:m) pure ester, respectively, for each Raman shift ω, and $M_{n:m}$ gives the (n:m) ester percentage (in weight) in the mixture. Fig. 7 compares different mixtures of esters using the (16:0), (18:0), (18:1), (18:2) and (18:3). Binary [(a) and (b)], ternary (c), quaternary (d) and fivefold (e) mixtures are presented. The spectra in Fig. 7 show that it is possible to obtain the spectrum of any mixture from the sum of the pure ester based on weighted averages according to the proportions in the real mixtures. Based in the spectra of the pure esters constituents, it is then possible to obtain the protocol according to the Eq. (1) to represent any mixture.

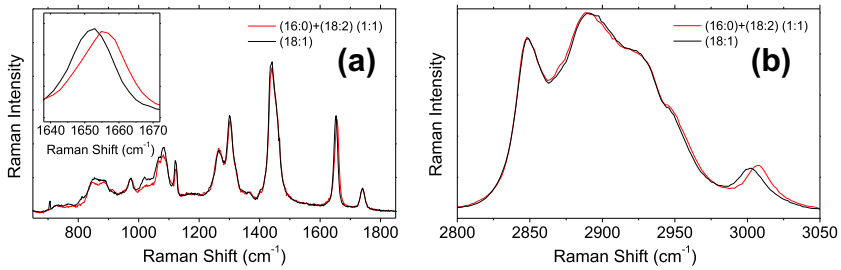

Fig. 6. Comparison between the Raman spectrum of (18:1) and the Raman spectrum of a 1:1 mixture of (18:2) + (16:0) (2 × 50 in Table 2). The (a) and (b) are two different spectral regions. The inset to (a) shows a zoom of the shift in the ~1650 cm^{-1} band.

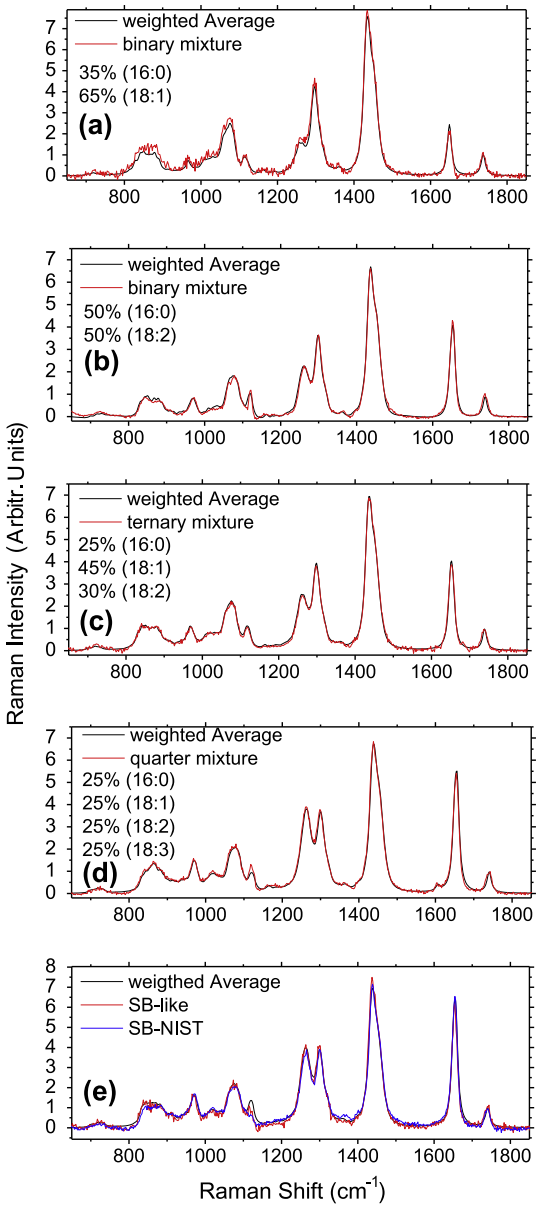

Fig. 7. Binary [(a) and (b)], ternary (c), quaternary (d) and fivefold mixtures (e). Red curves represent the spectra of physical mixtures. Black curves represent the respective weighted average of pure esters based on Eq. (1). Blue curve in (e) represent the spectrum of SB-NIST. (For interpretation of the references to colour in this figure legend, the reader is referred to the web version of this article.)

Fig. 7e shows the similarity between the mixture SB-like and SB-NIST (NIST standard). The combination of the ester type and the proportion of each ester in the solution determines the formation of the Raman spectra of different solutions. Beyond esters, biodiesel contains natural antioxidants such as tocopherois that have no contribution to the Raman spectrum. This can be confirmed when comparing the spectra of the pure ester mixture with that from the soybean biodiesel.

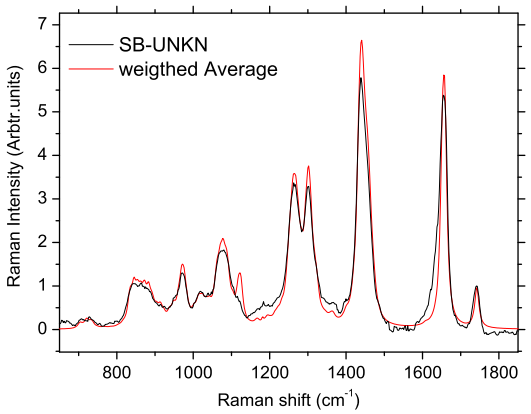

Fig. 8. Raman spectrum for SB-UNKN (black curve) as compared to the weighted average spectrum of pure esters based on Eq. (1), according to the percentage composition given in Table 2 for the SB-UNKN.

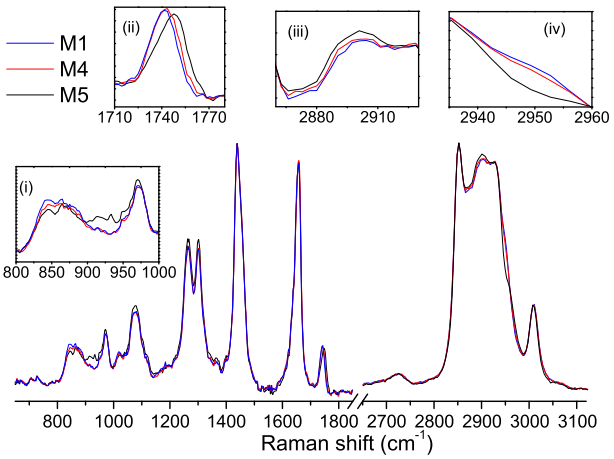

Fig. 9. Raman spectra for pure SB-UNKN (blue), pure soybean oil (black), and a mixture of both (red) (M1, M5 and M4, respectively, in Table 3). Insets (i)–(iv) highlights spectral regions where differences are clearly observed. (For interpretation of the references to colour in this figure legend, the reader is referred to the web version of this article.)

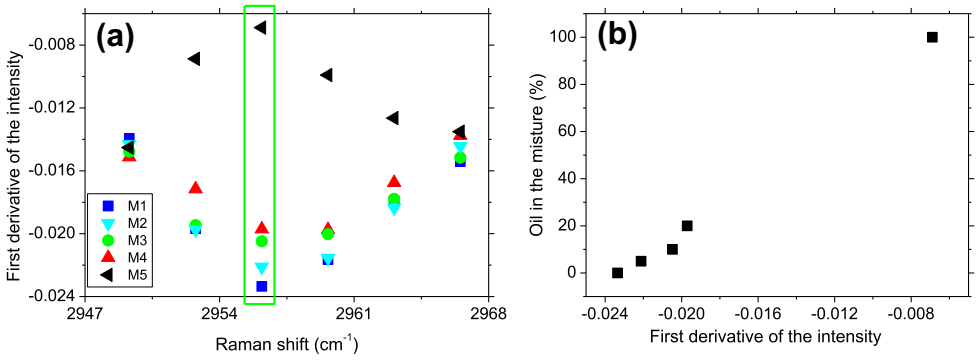

Fig. 10. (a) Values for the first derivatives for the five mixtures of soyabean oil and biodiesels listed in Table 3 within the spectral region between 2947 cm^{-1} and 2968 cm^{-1}. (b) Correlation between the percentage of soybean oil in the mixture and the first derivative of the Raman intensities at 2956 cm^{-1}.

3.3. Raman spectra of unknown and adulterated soybean biodiesel

In the previous sections, the possibility to differentiate ester solutions through their Raman spectra has been demonstrated. Here some aspects related to the application of this method to unknown samples, including adulterated biodiesels, are discussed.

The protocol using Eq. (1) relies on a measurement that is calibrated in both frequency and intensity. To determine the ester composition of a unknown soybean biodiesel sample using a different spectrometer, the SB-NIST has to be used to calibrate the measurement system. Fig. 8 shows the comparison of the standard-calibrated Raman spectrum of an initially unknown soybean biodiesel (SB-UNKN) and a spectral average according to the percentage composition for SB-UNKN listed in Table 2, built using Eq. (1). It is clear that only considering the 5 esters listed in Table 2, discrepancies in some peak intensities that go up to about 10% are observed. This result is in perfect agreement with the presence of 10.45% of different esters in this sample (see Table 2). Therefore, the analysis of unknown biodiesel samples requires the use of a complete set of calibrated ester spectra.

Fig. 9 illustrates the effect of biodiesel adulteration, by comparing the Raman spectra from the pure SB-UNKN (blue curve), pure biodiesel oil (black curve), and a mixture of both (red curve), spectra from mixtures M1, M4 and M5 listed in Table 3, respectively. The insets (i)–(iv) focus on specific spectral regions where the presence of oil can be identified and quantified. For example, inset (ii) shows the different Raman shift for the carbonyl band (C═O), appearing at 1740 cm^{-1} for mixture M1 and at 1747 cm^{-1} for mixture M5. The inset (iv) shows differences in the Raman intensities observed near 2950 cm^{-1}, discussed below.

These effects are known from literature [14,19], providing different methods for quantifying such type of adulteration. For example, Fig. 10a shows a plot that compares the first derivative of the spectra intensity form the five mixtures listed in Table 3, taking five points in the spectral region between 2947 cm^{-1} and 2968 cm^{-1}. This spectra region is chosen for showing important changes with the percentage of oil in the mixture (see inset (iv) in Fig. 9), the first derivative being maximum near 2956 cm^{-1}. Fig. 10b shows a correlation between first derivative at 2956 cm^{-1} and the percentage of soybean oil in the biodiesels. This linear correlation can be used to quantify adulteration of biodiesel by oil.

4. Conclusions

Here we demonstrate that the ester composition of biodiesels can be determined by using Raman spectroscopy. The protocol involves the determination of the full set of spectral parameters for the 3*N*-6 vibrational modes of each ester in the sample, where *N* is the number of atoms in each molecule.

While some characteristic Raman peak intensities are proportional to the number of unsaturations per molecule in the sample and can be used to differentiate esters with different number of unsaturations, in a mixture of esters, the peak intensities give the average number of unsaturations and cannot differentiate between, for example, two (18:1) molecules vs. one (16:0) molecule mixed with one (18:2) molecule. However, when the frequencies are considered, the uncertainties are reduced.

Biodiesels produced from different biomaterials are known to be different with respect to the different combination of ester types and the proportion of each ester in the solution [8,11,28]. Our protocol can, therefore, be used for determining the bio-origin of an unknown biodiesel. Furthermore, it is likely that distinct soil and climate conditions would generate differences in the final constitution of a given biodiesel. In this sense, our protocol might be applicable also in the determination of the geographical origin of a given biodiesel. However, to use this methodology in unknown samples, a full set of calibrated esters is necessary.

If adulteration of biodiesel by addition of vegetable oils or biodiesel degradation due to improper storage are to be tested, special caution is necessary, and specific methods can be used (e.g. Refs. [14,19] and Section 3.3). In any case, the importance of a standard biodiesel sample and a protocol, such as the one developed here, are demonstrated.

Acknowledgments

This work is supported by the CNPq, FAPEMIG, FAPERJ and INMETRO.

References

[1] Almeida EWC, Dos Santos HF, Miranda AM, Jorio A, Ferreira EHM, Achete CA, et al. Estudo teórico e experimental de espectros infravermelho de ésteres de ácido graxo presentes na composição do biodiesel de soja. Quim Nova 2012;35:1752–7.
[2] Goldemberg J. Ethanol for a sustainable energy future. Science 2007;315:808–10.
[3] Ayhan D. Competitive liquid biofuels from biomass. Appl Energy 2011;88:17–28. http://dx.doi.org/10.1016/j.apenergy.2010.07.016.
[4] Luque R, Davila LH, Campelo JM, Clark JH, Hidalgo JM, Luna D, et al. Biofuels: a technological perspective. Energy Environ Sci 2008;1:542–64.
[5] Kill King Corn. Nature 2007;449:637.
[6] Knothe G. Biodiesel Derived from a model oil enriched in palmitoleic acid, macadamia nut oil. Energy Fuel 2010;24:2098–103.
[7] Knothe G, Cermak SC, Evangelista RL. Cuphea oil as source of biodiesel with improved fuel properties caused by high content of methyl decanoate. Energy Fuel 2009;23:1743–7.
[8] Monteiro MR, Ambrozin ARP, Liao LM, Ferreira AG. Critical review on analytical methods for biodiesel characterization. Talanta 2008;77:593–605.

[9] Knothe G, Steidley KR. Kinematic viscosity of biodiesel fuel components and related compounds. Influence of compound structure and comparison to petrodiesel fuel components. Fuel 2005;84:1059–65.
[10] Wadumesthrige K, Ara M, Salley SO, Simon Ng KY. Investigation of lubricity characteristics of biodiesel in petroleum and synthetic fuel. Energy Fuel 2009;23:2229–34.
[11] Karmakar A, Karmakar S, Mukherjee S. Properties of various plants and animals feedstocks for biodiesel production. Bioresour Technol 2010;101:7201–10.
[12] BOLETIM MENSAL DE BIODIESEL, Setembro de 2010. <http://www.anp.gov.br>.
[13] Knothe G. Improving biodiesel fuel properties by modifying fatty ester composition. Energy Environ Sci 2009;2:759–66.
[14] Ghesti GF, Macedo JL, Braga VS, Souza ATCP, Parente VCI, Figueredo ES, et al. Application of raman spectroscopy to monitor and quantify ethyl esters in soybean oil transesterification. JAOCS 2006;83:597–601.
[15] Balabin RM, Safieva RZ. Biodiesel classification by base stock type (vegetable oil) using near infrared spectroscopy data. Anal Chim Acta 2011;689:190–7.
[16] Beattie JR, Bell SEJ, Moss BW. A critical evaluation of raman spectroscopy for the analysis of lipids; fatty acid methyl esters. Lipids 2004;39:407–19.
[17] Zerbi G, Conti G, Minoni G, Pison S, Bigotto A. Premelting phenomena in fatty acids: an infrared and Raman study. J Phys Chem 1987;91:2386–93.
[18] Santos Jr VO, Oliveira FCC, Lima DG, Petry AC, Garcia E, Suarez PAZ, et al. A comparative study of diesel analysis by FTIR FTNIR and FT-Raman spectroscopy using PLS and artificial neural network analysis. Anal Chim Acta 2005;547:188–96.
[19] Oliveira FCC, Brandao CRR, Ramalho HF, Costa LAF, Suarez PAZ, Rubim JC. Adulteration of diesel/biodiesel blends by vegetable oil as determined by Fourier transform (FT) near infrared spectrometry and FT-Raman spectroscopy. Anal Chim Acta 2007;587:194–9.
[20] Ministerio das Minas e Energia, Lei No. 11.097 de 13 de Janeiro de 2005; 2005, <http://www.mme.gov.br>.
[21] Guedes MLSAI, Alcantara, Jr. P, Moreira SGC, Barbosa Neto NM, Correa DS, Zilio SC. Characterization of buriti (Mauritia flexuosa L.) oil by absorption and emission spectroscopies. J Braz Chem Soc 2005;16:1113–7.
[22] Farhad SFU, Abedin KM, Islam MR, Talukder AI, Haider AFMY. Determination of ratio of unsaturated to total Fatty Acids in edible oils by laser Raman. J Appl Sci 2009;9(8):1538–43.
[23] Lewis EN, Bittman R, Levin IW. Methyl group substitution at C(1), C(2) or C(3) of the glycerol backbone of a diether phosphocholine: a comparative study of bilayer chain disorder in the gel and liquid-crystalline phases. Biochim Biophys Acta 1986;861:44–52.
[24] Batenjany MM, OLeary TJ, Levin IW, Mason JT. Packing characteristics of two-component bilayers composed of ester-and ether-linked phospholipids. Biophys J 1997;72:1695–700.
[25] Brown KG, Bicknell-Brown E, Ladjadj M. Raman-active bands sensitive to motlon and conformation at the chain termini and backbones of alkanes and lipids. J Phys Chem 1987;91:3436–42.
[26] Oakes RE, J.Beattie JR, Moss BW, Bell SEJ. DFT studies of long-chain FAMEs: theoretical justification for determining chain length and unsaturation from experimental Raman spectra. J Mol Struct (Theochem) 2003;626:27–45.
[27] Oakes RE, Beattie JR, Moss BW, Bell SEJ. Conformations, vibrational frequencies and Raman intensities of short-chain fatty acid methyl esters using DFT with 6-31G(d) and Sadlej pVTZ basis set. J Mol Struct (Theochem) 2002;586:91–110.
[28] Knothe G, Gerpen JV, Krahl J. The biodiesel handbook. Champaign: American Oil Chemists Society Press; 2005.
[29] Standard Reference Material®2772 B100 Biodiesel (Soy-Based), certificate of analysis, NIST, <http://www.nist.gov/srm>.
[30] Mohamadi F, Richards NGJ, Guida WC, Liskamp R, Lipton M, Caufield C, et al. Macromodel – an integrated software system for modeling organic and bioorganic molecules using molecular mechanics. J Comput Chem 1990;11:440.
[31] Weiner SJ, Kollman PA, Case DA, Singh UC, Ghio C, Alagona G, et al. A new force field for molecular mechanical simulation of nucleic acids and proteins. J Am Chem Soc 1984;106:765–84.
[32] Cornell WD, Cieplak P, Bayly CI, Gould IR, Merz Jr KM, Ferguson DM, et al. A second generation force field for the simulation of proteins, nucleic acids, and organic molecules. J Am Chem Soc 1995;117:5179–97.
[33] Frisch GWTMJ, Schlegel HB, Scuseria GE, Robb MA, Cheeseman Jr., Montgomery JA, et al., Revision C.2a ed.; 2004.
[34] Ochterski JW. Vibrational analysis in Gaussian. Wallingford: Gaussian; 1999. <http://www.gaussian.com/g$_w$hitepap/vib.htm>.
[35] Dos Santos HF, Almeida WB, Val AMG, Guimaraes AC. A semiempirical infrared spectrum of the 3-phenyl – 1,2,3-oxathiazolidine 2-oxide. Quim Nova 1999;22:732–6.
[36] Tfayli A, Guillard E, Manfait M, Guffroy AB. Thermal dependence of Raman descriptors of ceramides. Part I: Effect of double bonds in hydrocarbon chains. Anal Bioanal Chem 2010;397:1281–96.
[37] Neuberta R, Rettig W, Wartewig S, Wegener M, Wienhold A. Structure of stratum corneum lipids characterized by FT-Raman spectroscopy and DSC II. Mixtures of ceramides and saturated fatty acids. Chem Phys Lipids 1997;89:3–14.
[38] Silverstein RM, Webster FX, Kiemle DJ. Spectrometric identification of organic compounds. 7th ed. John Wiley and Sons, Inc.; 2006.
[39] Socrates G. Infrared and Raman characteristic group frequencies: tables and charts. 3rd ed. Wiley; 2000.